Contents lists available at ScienceDirect

Applied Energy

journal homepage: http://ees.elsevier.com

Techno-economic evaluation of biomass-to-fuels with solid-oxide electrolyzer

Hanfei Zhang [a], Ligang Wang [b,c,*], Jan Van herle [b], François Maréchal [c], Umberto Desideri [a,*]

[a] Department of Energy, Systems, Territory and Constructions Engineering, University of Pisa, Pisa, Italy
[b] Group of Energy Materials, Swiss Federal Institute of Technology in Lausanne (EPFL), Sion, Switzerland
[c] Industrial Process and Energy Systems Engineering, Swiss Federal Institute of Technology in Lausanne (EPFL), Sion, Switzerland

ARTICLE INFO

Keywords
Biomass gasification
Biomass-to-fuel, power-to-liquid, power-to-gas
Energy storage
Solid-oxide electrolyzer

ABSTRACT

Thermochemical biomass-to-fuel conversion requires an increased hydrogen concentration in the syngas derived from gasification, which is currently achieved by water–gas-shift reaction and CO_2 removal. State-of-the-art biomass-to-fuels convert less than half of the biomass carbon with the remaining emitted as CO_2. Full conversion of biomass carbon can be achieved by integrating solid-oxide electrolyzer with different concepts: (1) steam electrolysis with the hydrogen produced injected into syngas, and (2) co-electrolysis of CO_2 and H_2O to convert the CO_2 captured from the syngas. This paper investigates techno-economically steam- or co-electrolysis-based biomass-to-fuel processes for producing synthetic natural gas, methanol, dimethyl ether and jet fuel, considering system-level heat integration and optimal placement of steam cycles for heat recovery. The results show that state-of-the-art biomass-to-fuels achieve similar energy efficiencies of 48–51% (based on a lower heating value) for the four different fuels. The integrated concept with steam electrolysis achieves the highest energy efficiency: 68% for synthetic natural gas, 64% for methanol, 63% for dimethyl ether, and 56% for jet fuel. The integrated concept with co-electrolysis can enhance the state-of-the-art energy efficiency to 66% for synthetic natural gas, 61% for methanol, and 54% for jet fuel. The biomass-to-dimethyl ether with co-electrolysis only reaches an efficiency of 49%, due to additional heat demand. The levelized cost of the product of the integrated concepts highly depends on the price and availability of renewable electricity. The concept with co-electrolysis allows for additional operation flexibility without renewable electricity, resulting in high annual production. Thus, with limited annual available hours of renewable electricity, biomass-to-fuel with co-electrolysis is more economically convenient than that with steam electrolysis. For a plant scale of 60 MW_{th} biomass input with the renewable electricity available for 1800 h annually, the levelized cost of product of biomass-to-synthesis-natural-gas with co-electrolysis is 35 $/GJ, 20% lower than that with steam-electrolysis.

Nomenclature

Abbreviations

AAHs	annual available hours of renewable electricity
AE	alkaline electrolyzer
AGR	acid gas removal
AOH	annual operating hours
ASU	air separation unit
BCE-FUEL	biomass-to-fuel with co-electrolysis
BSE-FUEL	biomass-to-fuel with steam electrolysis
BtDME	biomass-to-dimethyl ether
BtF	biomass-to-fuel
BtJF	biomass-to-jet fuel
BtL	biomass-to-liquid
BtMeOH	biomass-to-methanol
BtSNG	biomass-to-synthetic natural gas
CE	co-electrolysis
DME	dimethyl ether
EFG	entrained flow gasifier
FT	Fischer-Tropsch
HTFT	high-temperature Fischer-Tropsch
HTSR	high-temperature water–gas shift reactor
HEN	heat exchanger network
HHV	higher heating value
IEA	international energy agency
JF	jet fuel
LHV	lower heating value
LTFT	low -temperature Fischer-Tropsch
LTSR	low-temperature water–gas shift reactor

* Corresponding authors at: Group of Energy Materials, Swiss Federal Institute of Technology in Lausanne (EPFL), Switzerland (L. Wang).
E-mail addresses: ligang.wang@epfl.ch (L. Wang); umberto.desideri@unipi.it (U. Desideri)

https://doi.org/10.1016/j.apenergy.2020.115113
Received 16 February 2020; Received in revised form 21 April 2020; Accepted 28 April 2020
Available online xxx

MeOH	methanol
MSW	municipal solid waste
MtG	methanol-to-gasoline
PEME	polymer electrolyte membrane electrolyzer
PtH	power-to-hydrogen
SE	steam electrolysis
SNG	synthetic natural gas
SoA-FUEL	State-of-the-art biomass-to-fuel
SOE	solid-oxide electrolysis
STN	steam turbine network
TIGAS	topsoe integrated gasoline
WGSR	water–gas-shift reaction
$	united states dollar
€	euro

Greek symbols

η	energy efficiency

Mathematical symbols

CAPEX	capital expenditure
C_{dep}	depreciation cost
C_{inv}	investment cost
C_{opt}	operational cost
C_{rev}^{byp}	byproduct revenue
i	annual interest rate
LCOP	levelized cost of the product
M	syngas modular
$\dot{M}_{\text{product}}$	the mass flow of obtained product
$\dot{M}_{\text{Biomass}}$	the mass flow of biomass feed
MPSP	minimum product selling price
$\Delta\dot{E}^{+}$	net electric power input
$\Delta\dot{E}^{-}$	net electric power output
ΔH_{298K}	standard enthalpy of formation, kJ mol^{-1}
OPEX	operational expenditure
T	temperature, K

Superscripts

n	project lifetime

1. Introduction

A large amount of fossil fuels is currently used to generate electricity and produce gaseous or liquid fuels, leading to severe problems of fossil-fuel shortage and climate change [1–3]. Coping with these issues requires the energy mix being adjusted by increasing the penetration of renewable energies [4]. Biomass, as an alternative source, accounts for 14% of the global renewable energy [5,6]. Biomass can be utilized to generate heat, electricity, and gaseous or liquid fuels in a carbon–neutral way [7–9]. The increased use of biomass allows for the potential of carbon-free production of the secondary energy.

Biomass can be converted to various fuels (namely biomass-to-fuel (BtF)) via thermochemical routes based on gasification. The biomass gasification technologies mainly include moving-bed (425–650 °C at atmospheric pressure), fluidized-bed (800–950 °C, 1–5 bar), or entrained-flow (600–1200 °C and 1–80 bar) [10,11]. Compared with moving-bed and fluidized-bed gasification technologies, entrained-flow gasifiers (EFG) have been widely used in coal gasification for integrated-gasification combined cycles [12,13] and coal-to-fuels, which has a high oxygen demand but enables very high reaction rates and conversion of biomass into syngas with low methane, low CO_2 [14] and almost no tar and gaseous hydrocarbons [15,16]. Syngas production with oxygen instead of air and under high pressure leads to a compact design of downstream equipment, and reduces or even avoids power consumption of syngas compression for fuel synthesis [11].

The state-of-the-art biomass-to-fuel (SoA-FUEL) process, the chemical synthesis of fuels, requires a higher stoichiometric hydrogen-to-carbon molar ratio (2–3) of syngas; however, the syngas derived from biomass gasification is hydrogen deficient with low hydrogen-to-carbon ratio (below 1). Hence, syngas composition needs to be adjusted by reducing the carbon fraction and increasing the hydrogen content, which can be achieved by employing the water–gas-shift reactor (WGSR) with the result of an increased CO_2 concentration. More than half of biomass carbon ends up into CO_2 [17] and needs to be removed via an acid gas removal (AGR) process, e.g., amines-based chemical absorption [18]. Potential fuel products include synthetic natural gas (SNG), methanol (MeOH), dimethyl ether (DME), and Fischer-Tropsch (FT) fuels (i.e., jet fuel (JF) and gasoline). The process design of wood-to-SNG investigated in Ref. [19] reported a thermal efficiency of 58% based on the lower heating value (LHV) and a low overall carbon conversion of 35%. Different technologies for liquid fuel production from lignocellulosic biomass studied in Ref. [7] concluded similar overall biomass-to-liquid (BtL) efficiencies (LHV), i.e., 51.3% (crude FT fuel), 52.5% (MeOH), and 53.5% (DME). These efficiencies are higher than those reported in Ref. [20] from 37.9% to 47.6% (LHV), depending on the synthesis technologies, e.g., FT synthesis, methanol to gasoline (MtG) or the Topsoe Integrated Gasoline (TIGAS) synthesis. Similar efficiency numbers (40–45%, HHV) have been reported for biomass-to-FT liquids in Ref. [21].

To deal with the low carbon utilization in the SoA-FUEL process, an alternative is injecting green hydrogen into the syngas derived from biomass gasification to increase the H/C ratio, so that the biomass carbon could be fully converted to fuels without WGSR and AGR. Green hydrogen is mainly produced via H_2O electrolysis driven by renewable power with the by-product, i.e., high purity oxygen, used as the gasification agent. In this way, the expensive and energy-intensive cryogenic air separation unit (ASU) can be avoided [17,22]. A big potential is predicted for such power-to-fuels processes, and it has been predicted that nearly half of total ammonia and two-thirds of methanol will be produced via electrolysis by 2050 [23]. The core of green hydrogen production is electrolysis technology. Comparing with low-temperature electrolysis technologies, high-temperature solid-oxide electrolysis (SOE) is more advantageous to couple with biomass-to-fuels, because of (1) higher electrical efficiency with steam electrolysis, (2) enhanced system-level heat integration by utilizing waste heat from gasification process to generate steam for SOE [24], thus resolving the bottleneck of enhancing system efficiency of power-to-hydrogen. Such benefits have been proven by coupling SOE with biomass-to-SNG and municipal solid waste (MSW)-to-SNG, achieving LHV system efficiencies of 70% [25] and 67% [26], respectively. Compared with conventional processes with WGSR and AGR but no SOE, the coupling of SOE with biomass-to-MeOH and -FT liquids can enhance the system efficiency by 13 [11] and 6 [27] percentage points, respectively. Although the integrated systems achieve higher efficiency, it is greatly affected by the availability of renewable electricity: When renewable electricity is not accessible, the whole system needs to be shut down. This might be overcome by the co-electrolysis-based biomass-to-fuels, in which the CO_2 captured in the SoA-FUEL process is sent to the SOE together with steam to produce syngas for the downstream synthesis process. This co-electrolysis-based concept is flexible for full carbon conversion: When renewable electricity is not available, the system switches to the SoA-FUEL process with the CO_2 captured and stored, which could be converted when renewable electricity is available.

In this study, two concepts for full biomass carbon conversion are proposed by integrating SOE: (1) biomass-to-fuel with steam electrolysis (BSE-FUEL) and (2) biomass-to-fuel with co-electrolysis (BCE-FUEL). The first concept operates the SOE with steam electrolysis (SE) to re-

place the WGSR and AGR, with the SOE sized by the hydrogen flow required for full carbon conversion. The second concept operates the SOE with co-electrolysis to convert the captured CO_2 from the state-of-the-art biomass-to-fuel processes to the target fuels. The direct co-electrolysis of syngas is not considered in this paper due to the deep syngas cleaning needed for the SOE, and it is also assumed that, with cost- and energy-intensive amines-based CO_2 capture, the levels of impurities in the CO_2 stream are below the tolerance of the SOE. Particularly, employing only direct co-electrolysis of syngas asks for high availability of renewable electricity, which can hardly be possible in practice.

The two integration concepts (BSE-FUEL and BCE-FUEL) of SOE-based biomass-to-fuels are techno-economically evaluated and compared with the SoA-FUEL plants for various products, i.e., SNG, MeOH, DME, and JF via FTS. The operational flexibility of the two SOE-based biomass-to-fuel processes is investigated considering the intermittent nature of renewable electricity. The rest of the paper is organized as follows: the processes involved are described and modelled in Section 2. In Section 3, the methodology is introduced with a detailed definition of thermodynamic and economic performance. Afterward, the thermodynamic and economic performances of the studied cases are discussed comprehensively in Section 4 to support the practical process design. The conclusions are drawn in Section 5.

2. Biomass-to-fuels

The systems investigated are based on EFG for gaseous and liquid fuels, i.e., SNG, MeOH, DEM, and JF with the SOE supplying hydrogen (steam electrolysis)/syngas (co-electrolysis), oxygen, and additional capability of enhancing heat utilization.

2.1. System description

2.1.1. Biomass-to-SNG (BtSNG)

(1) State-of-the-art biomass-to-SNG (SoA-SNG)

The SoA SNG plant with EFG, WGSR, and AGR is illustrated in Fig. 1. The biomass feedstock (1) is first fed into an EFG using pure oxygen (5) as oxidant agent, which is supplied by an ASU. The obtained syngas (7) is cooled down to 290 °C and then divided into two streams: stream (9) enters the WGSR to increase the H_2 content, and the bypass stream (10) is mixed with (14). Part of the CO_2 in syngas (16) is removed via monoethanolamine (MEA) based chemical absorption to reach a desired syngas molar modular number, which is defined as $(H_2 - CO_2)/(CO + CO_2)$. For the synthesis of SNG described in [28] in detail, the hydrogen-rich syngas (27) with the module number of 3 [28,29] is converted by isothermal methanation reactors (290 °C, 25 bar) for enhanced single-pass conversion [30,31]. The exothermic methane synthesis involves two global reactions (Eqs. (1) and (2)) with the catalyst Ni/Al_2O_3 [28,32]:

$$CO + 3H_2 \leftrightarrow CH_4 + H_2O \quad -\Delta H_{298K} = 206 \text{ kJ/mol} \tag{1}$$

$$CO_2 + 4H_2 \leftrightarrow CH_4 + 2H_2O \quad -\Delta H_{298K} = 165 \text{ kJ/mol} \tag{2}$$

Raw methane is then upgraded to grid-quality SNG, compressed further for grid injection. The network requirement of Zhejiang Province in China is 34.2 MJ/Nm^3 (LHV), 94 vol% of CH_4, 37–42 bar.

(2) Biomass-to-SNG with steam electrolysis (BSE-SNG)

The BSE-SNG system is illustrated in Fig. 2. Biomass is fed to the EFG with syngas produced and cleaned afterward. For adjusting the syngas composition, hydrogen is produced via the SOE with the following process: Demineralized water (5) is vaporized and superheated (7) to be mixed with cathode recirculation (13) as the reactant feed and sent to the cathode to produce H_2. The cathode recirculation (13) is to keep the reduction atmosphere to avoid re-oxidation of Ni-YSZ [34]. The electrolysis by-product, O_2, is swept by pure oxygen flow, which offers additional ability for thermal management of the stack. The oxygen recirculation (15) allows the stack for a higher current density, thus resulting in a larger production capacity [35–38]. The produced oxygen (18) is then compressed and supplied to the EFG with extra O_2 (21) as a final by-product. The hydrogen (23) is compressed, cooled and mixed with the syngas (4). The SOE is sized to ensure that the gas composition (26) reaches the requirement of the downstream fuel synthesis.

(3) Biomass-to-SNG with co-electrolysis (BCE-SNG)

The BCE-SNG system is illustrated in Fig. 3. The CO_2 captured in the SoA plant is sent into the SOE to produce syngas by co-electrolysis of CO_2 and H_2O. The SOE is sized by the available CO_2 captured from the syngas after the water–gas-shift reactor. Such a system can enhance the carbon conversion compared with the SoA case and the flexibility of the whole plant: When renewable electricity is not available, the plant can still work with water–gas-shift reactor and CO_2 removal (the SoA mode) with the captured CO_2 stored for the period with available renewable electricity.

2.1.2. Biomass-to-MeOH (BtMeOH)

The molar module number $M = (H_2 - CO_2)/(CO + CO_2)$ of the hydrogen-rich syngas for methanolization is at around 2.0 [11]. Methanol synthesis is less exothermic than methane synthesis. The major reactions (Eqs. (3) and (4)) with the catalyst $Cu/ZnO/Al_2O_3$ [39–41] are

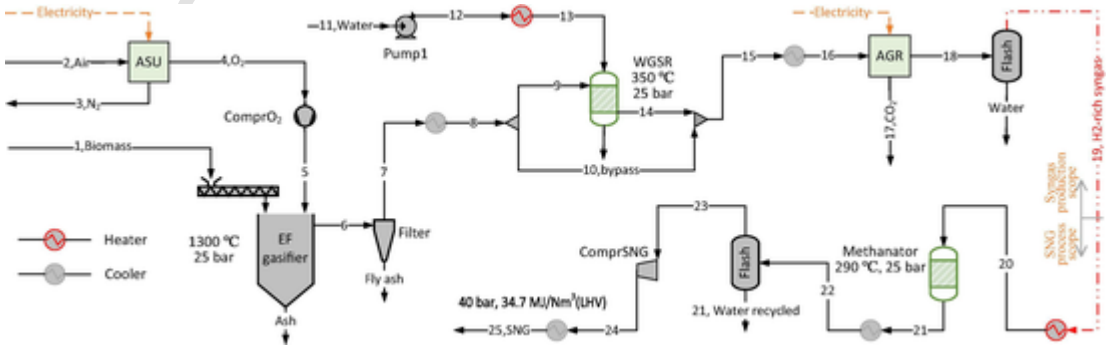

Fig. 1. Schematic of the state-of-the-art biomass-to-synthetic natural gas system with EFG, single-stage high-temperature WGSR, ASU (cryogenic distillation) and AGR (MEA-based CO_2 removal). The heat exchanger network (HEN) is not explicitly designed but its performance is estimated via the classical chemical engineering approach described elsewhere, e.g. [33]. The Rankine cycle (steam turbine network (STN)) is not explicitly presented but is optimally placed and sized for heat recovery.

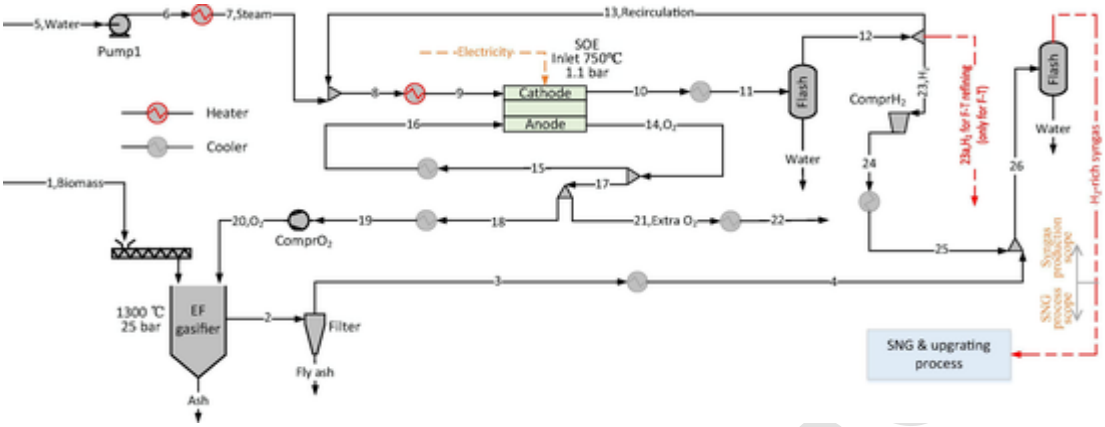

Fig. 2. Schematic of the biomass-to-synthetic natural gas system with steam electrolysis. The synthetic natural gas, the Rankine cycle and the heat exchanger network are handled in the same way as described in Fig. 1.

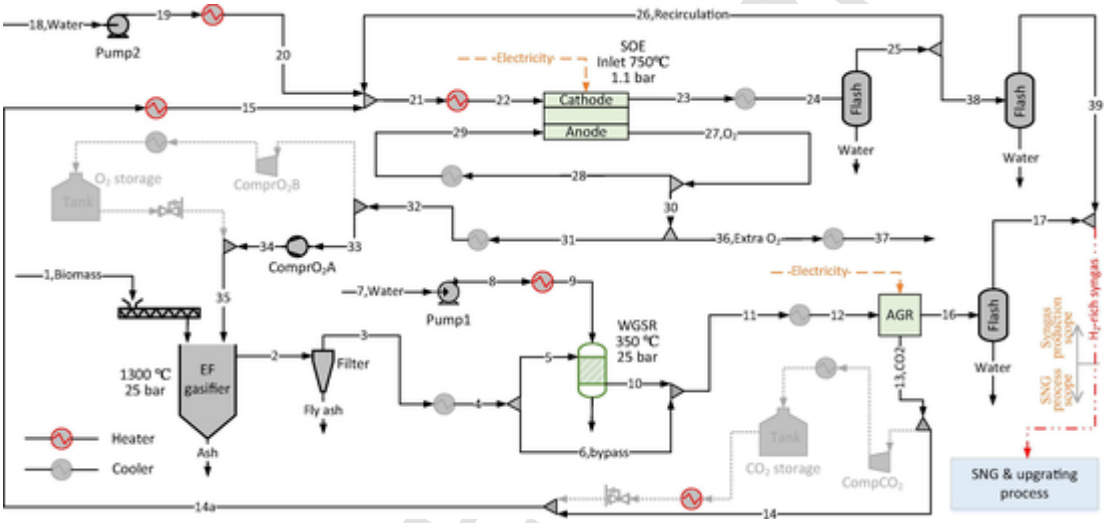

Fig. 3. Schematic of the biomass-to-synthetic natural gas system with co-electrolysis. The synthetic natural gas, the Rankine cycle and the heat exchanger network are handled in the same way as described in Fig. 1.

CO and CO_2 methanolization:

$$2H_2 + CO \leftrightarrow CH_3OH \quad -\Delta H_{298K} = 90.64 \text{ kJ/mol} \tag{3}$$

$$3H_2 + CO_2 \leftrightarrow CH_3OH + H_2O \quad -\Delta H_{298K} = 41.17 \text{ kJ/mol} \tag{4}$$

The synthesis reactor considered in this paper is operated isothermally at 230 °C and 56 bar with more details given in [11,28]. Since the hydrogen-rich syngas production processes are the same as that in Figs. 1–3 with the syngas-to-methanol process illustrated in Fig. 4. The hydrogen-rich syngas is compressed and mixed with the recirculated gas (9). The stream (3) is further compressed to 56 bar and then heated to 200 °C, and finally sent to the methanol reactor. The reaction product (6) is cooled to 40 °C and fed (7) to a flash (Vapor-liquid separator). The gas stream (8) is compressed and recycled, with a small amount of the purge gas (10) to avoid the accumulation of inert gases and CH_4. The raw methanol (17) is depressurized and separated in an-

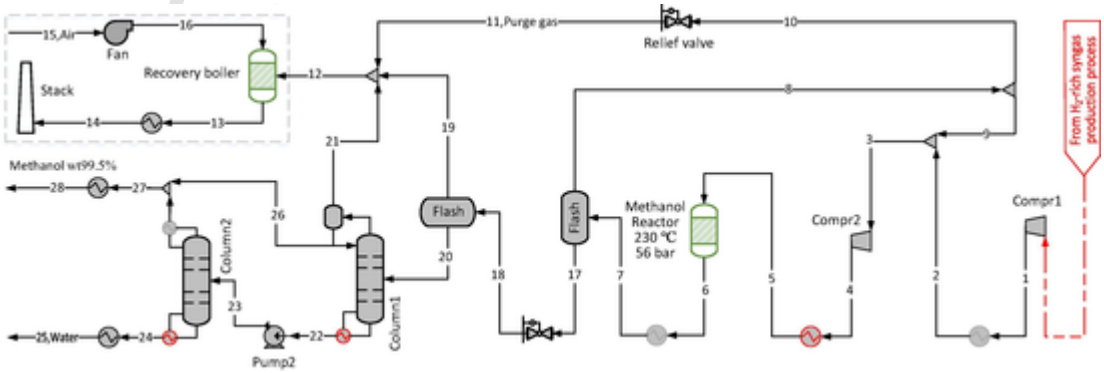

Fig. 4. Schematic of the methanol synthesis process. The hydrogen-rich syngas production processes illustrated in Figs. 1–3 are not repeated.

other flash drum to produce crude methanol (20), which is further upgraded to a high purity of 99.5 wt% with a two-stage distillation. The purge gas (11) and flash gas (19 & 21) are burnt with additional heat supplied to the remaining process.

2.1.3. Biomass-to-DME (BtDME)

The current commercially-available DME synthesis is the dehydration of methanol over a $\gamma - Al_2O_3$ catalyst [42–45]:

$$2CH_3OH \leftrightarrow CH_3OCH_3 + H_2O \quad -\Delta H_{298K} = 23 \text{ kJ/mol} \tag{5}$$

The methanol dehydration reaction is slightly-exothermic; thus it can be handled by an adiabatic reactor [28], normally operating at 250–400 °C and 20 bar [42] with the one-pass methanol conversion of 70–85% [28]. In this paper, the adiabatic reactor is assumed to be operated at 350 °C and 20 bar.

The process of methanol synthesis and dehydration to DME is illustrated in Fig. 5 with the methanol synthesis system already described in Section 2.1.2. Pure methanol (28) is pressurized and mixed with the recirculation (43). The mixture (30) is heated to 350 °C and sent to the DME reactor. Raw DME (33) undergoes two-stage distillation to reach a high purity of 99.6 wt%.

2.1.4. Biomass-to-Jet fuel (BtJF)

The FT synthesis is a highly exothermic polymerization reaction that converts CO and H_2 mixture into a range of hydrocarbons and water, as shown in Eq. (6) [46–48].

$$CO + 2H_2 \leftrightarrow -(CH_2) - +H_2O \quad -\Delta H_{298K} = 150 \text{ kJ/mol} \tag{6}$$

The main reactions during FT synthesis can be represented by Eqs. (7) and (8).

$$\text{Alkenes}: nCO + 2nH_2 \leftrightarrow (CH_2)n + nH_2O \tag{7}$$

$$\text{Alkanes}: nCO + (2n+1)H_2 \leftrightarrow H(CH_2)nH + nH_2O \tag{8}$$

Commercial technologies for the FT synthesis are usually classified into high-temperature FT (HTFT) and low-temperature FT (LTFT) synthesis at 20–45 bar [46,47,49]. The HTFT operates at 300–350 °C and is the most suitable for producing motor-gasoline and linear 1-olefins over a Fe-based catalyst with the H_2/CO mole ratio of 0.5–2.5. The LTFT operates at 200–240 °C and is favorable to produce long-chained hydrocarbons, i.e., kerosene and diesel based on Co-based catalysts, with the H_2/CO mole ratio of 2.0–2.3 [46–49] and a higher one-pass CO conversion of 70–90% [17,48,50,51]. The target product of this process is JF, so the LTFT synthesis with Co-based catalysts is adopted at 220 °C and 25 bar with the one-pass CO conversion of 80% [46,52,53].

The JF synthesis via the LTFT process is illustrated in Fig. 6. The hydrogen-rich syngas (1) with the H_2/CO mole ratio of 2 is mixed with the recirculated gas (8), which is then heated and sent to the FT reactor. The mainstream (4) from the FT reactor is cooled to 40 °C and then sent to (5) a flash drum to produce raw FT products (9). Afterward, the raw products (9) enter a complex JF upgrading process, during which the FT products (11) are first sent to column 1 to be separated as naphtha (29) and a mixture of wax and distillate (12). The naphtha (29) is pressurized and sent to the Oligomerization reactor (220 °C, 38 bar) over ZSM-5 catalysts to be converted mainly to distillate-range products [54,55]. The stream (33) out of the Oligomerization reactor is cooled and enters the column 2, with the light hydrocarbon (35) separated at the top as the by-product, and the motor-gasoline and distillate (38) separated at the bottom. The mixture of wax and distillate (12) is cooled and then fed into the column 3 to be separated into wax (14) and distillate (40). The wax (15) is pressurized and sent to the hydrocracking reactor (340 °C, 40 bar) for kerosene, naphtha, and paraffin products [46,54]. The reactor outlets (21) are cooled and enter the column 4 to obtain the JF (24). Light hydrocarbons are sent to the column 6 for the by-product motor-gasoline (28) and LPG. The distillate (38) and (41) are mixed and pressurized for the hydroisomerization reactor (355 °C, 60 bar) to hydrosaturate the olefins [53,56]. The reactor outlets (47) are cooled and enter the column 5 for kerosene range products (50) to be blended JF, and the stream (52) as a blending component of motor-gasoline. The purge gas (58) and flash gas (57) are burnt for energy recovery.

2.2. System modeling

The key components to be modelled for the system described in Section 2.1 are (1) the EFG, (2) the SOE, (3) the WGSR, (4) the AGR, (5) fuel synthesis reactors, (6) distillation for fuel upgrading, and (7)

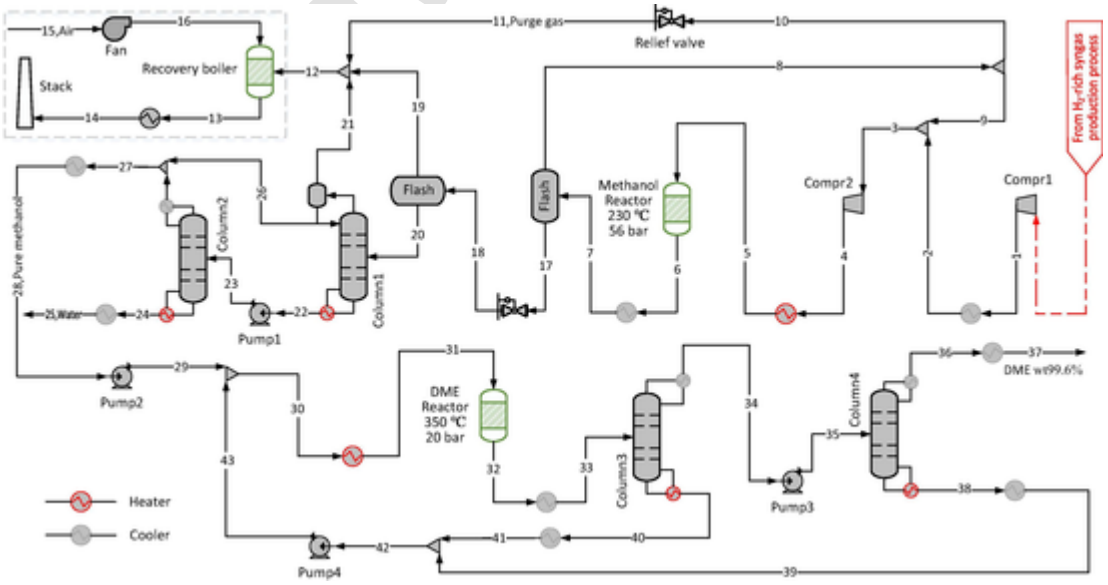

Fig. 5. Schematic of the DME synthesis process via methanol. The hydrogen-rich syngas production processes illustrated in Figs. 2 and 3 are not repeated.

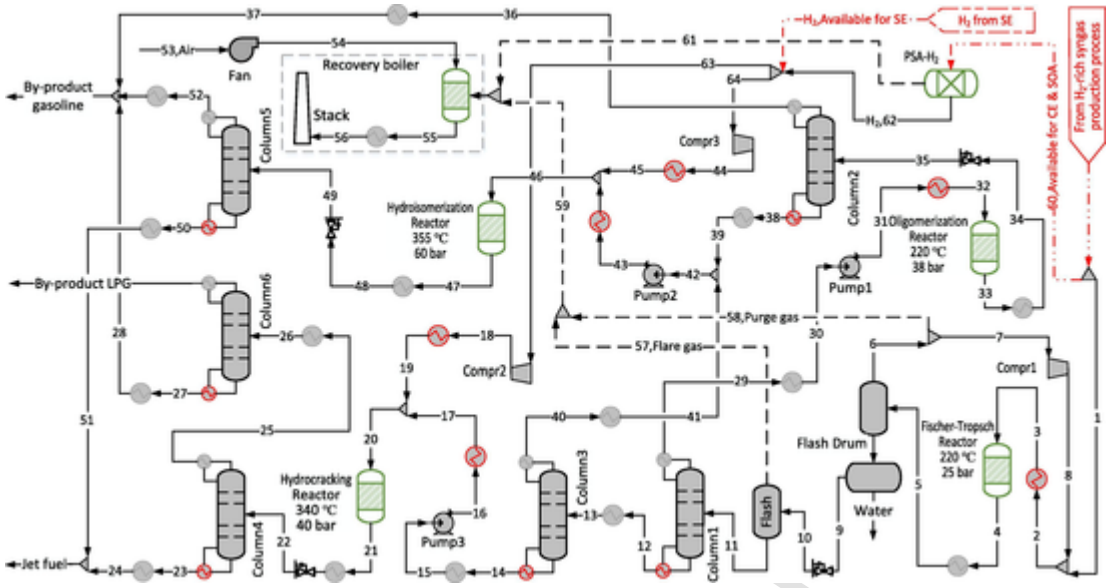

Fig. 6. Schematic of jet-fuel synthesis and purification via the FT process. The hydrogen-rich syngas production processes illustrated in Figs. 1–3 are not repeated.

heat-exchanger network and steam-turbine network. The models of EFG, SOE and fuel synthesis reactors (SNG, MeOH and DME) have been developed and discussed in detail in our previous studies [11,24,28,35,37,57]. The LTFT synthesis and upgrading are modeled based on Refs. [47,52–54]. The distribution of the LTFT crude products is referred to [58] with Table 1 for the JF refinery, which agrees well with those reported in Ref. [54]. The performance of the heat exchanger network is estimated with heat cascade calculation, as described elsewhere in Refs. [59–61]. The steam turbine network (STN) is employed for optimal heat recovery and has been well formulated in Refs. [62,63]. The compositions of the biomass (wood) are given in Table 2.

The operating windows of the stack have been studied in detail in our previous study [28]. In this work, the stack is selected to operate under the exothermic mode, and the corresponding operating parameters are shown in Table 3.

3. Methodology

The techno-economic evaluation is carried out using the in-house platform developed at EPFL, which can readily integrate the Aspen models developed and perform plant-wise heat integration to close the energy balance of the overall system. This platform has been employed to investigate the design of many complex systems, e.g. [24,28,35,37,64]. The detailed workflow of the evaluation is described below, following Refs. [11,35,64,65]:

(1) Process models are simulated to obtain the mass and energy flows of the considered process and also each equipment.
(2) Heat and mass integration, formulated in mixed integer linear programming problem, is performed mathematically with the selection and sizing of utilities to close the energy balance. The utilities considered here are mainly the electrical heater, syngas burner and steam turbine network.
(3) Classical hot–cold and grand composite curves are obtained for the interpretation of thermal integration. The minimum numbers, area and cost of the heat exchangers are estimated by the vertical heat transfer [33].
(4) The evaluation indicators, i.e., the system efficiency, levelized cost of the fuel produced, are then calculated following Sections 3.1 and 3.2.

Table 1
Product distribution from LTFT jet fuel refinery.

Products	Ref. [54] (mass %)	This work (mass %)
Fuel gas	7.4	7.0
Liquid petroleum gas	11.4	17.2
Gasoline	19.6	16.7
Jet fuel	57	58.6
Unrecovered organics	4.3	–
Water	0.3	0.2

3.1. System efficiency

The thermodynamic performance is determined in overall energy efficiency (η), which is defined as

$$\eta = \frac{\dot{M}_{\text{product}} \cdot LHV_{\text{product}} + \Delta E^{-}}{\dot{M}_{\text{biomass}} \cdot LHV_{\text{biomass}} + \Delta E^{+}} \cdot 100 \quad (9)$$

where $\dot{M}$ is the mass flow rate (kg/s). The superscripts – and + refer, respectively, to the net electricity produced (output) and consumed (input), $\Delta E = |E^{-} - E^{+}|$ [27]. Only one of the net electricity input ΔE^{+} and output ΔE^{-} occurs.

Table 2
The compositions of biomass.

Material	Ultimate analysis (air-dried, wt.%)					Proximate analysis (air-dried, wt.%)				Heating value (kJ/kg)
	C	H	O	N	S	Moisture	Ash	Volatile	Fixed carbon	LHV
Biomass [11]	48.88	6.29	33.59	1.7	0.06	4.79	4.69	72.29	18.23	18,313

Table 3
Practical stack operating point with the stack inlet temperature of 750 °C and 1 bar. The stack power is corresponding to 5120 cm^2 active cell area.

Operating variable	SE	CE-SNG	CE-MeOH/ DME	CE-JF
Average current density (A/ cm^2)	0.95	0.95	0.95	0.95
Average voltage (V)	1.36	1.38	1.40	1.41
Cathode feed H_2O/CO_2 (sccm/cm^2)	8/0	6.25/ 1.59	5.65/2.08	5.25/ 2.50
Reactant utilization (%)	80	80	80	80
Anode feed (sccm/cm^2)	20	20	20	20
Outlet temp. (°C)	836	823	825	825
Stack power (kW)	6.67	6.75	6.82	6.87

The heat and mass integration has been considered in the efficiency definition. For example, the integration of steam turbine network for recovering high- and intermediate-grade heat affects the net electricity input or output. The use of syngas burner as hot utility reduces the product production, which is eventually reflected in the efficiency number.

3.2. Levelized cost of the fuel production

Based on the capital expenditure (CAPEX) and operating expenditure (OPEX), the levelized cost of product LCOP ($/GJ) can be calculated according to [66]:

$$LCOP = \frac{C_{opt} + C_{dep} - C_{rev}^{byp}}{P_{product}} \quad (10)$$

where $P_{product}$ is the capacity of fuel production (GJ/year), C_{rev}^{byp} is the byproduct revenues ($/year), and C_{dep} is the depreciation cost ($/year). The C_{dep} can be calculated:

$$C_{dep} = C_{inv} \times \frac{i \times (i+1)^n}{(i+1)^n - 1} \quad (11)$$

where the C_{inv} is the investment cost ($), i is the annual interest rate and n is the plant lifetime (year). More information about CAPEX and OPEX has been given in Part A of the supplement material. The assumptions for the economic evaluation include a plant lifetime of 25 years [67], an interest rate of 10% [66], annual operating hours of 7200 h [67], an electricity price of 73 $/MWh [68], and a biomass price of 5.1 $/GJ [69].

4. Results and discussion

The biomass-to-SNG, MeOH, DME, and JF described in Section 2.1 are evaluated techno-economically and compared with the same biomass input in Sections 4.1 and 4.2. Section 4.3 further investigates the operational flexibility of the cases.

4.1. Thermodynamic performance

4.1.1. System energy efficiency

The overall system energy efficiency (LHV) of the BtFs is calculated with Eq. (10) in Section 3.1. The main influencing factors on system efficiency are (1) the type of biomass, (2) the stack operating point, (3) thermodynamic inefficiencies of fuel synthesis and upgrading, (4) system-level heat integration, and (5) heat recovery. The proposed BtF cases employ the same type of biomass and similar stack operating points. Therefore, the difference between the thermodynamic performances of different systems in Fig. 7 are mainly due to the factors (3), (4), and (5): The SoA cases reach an overall energy efficiency of 51% for SNG, 49% for MeOH, 48% for DME, 48% for JF. The efficiency numbers are similar, due to the employment of STN, which recovers the heat converted particularly from the exergy destructed from chemical reactions. The BSE cases have the highest energy efficiency (68% for SNG, 64% for MeOH, 63% for DME, 56% for JF). The integration of SoA and co-electrolysis (the BCE cases) improve the energy efficiency (66% for SNG, 61% for MeOH, 54% for JF) compared to the SoA cases except for the BCE-DME case (49%).

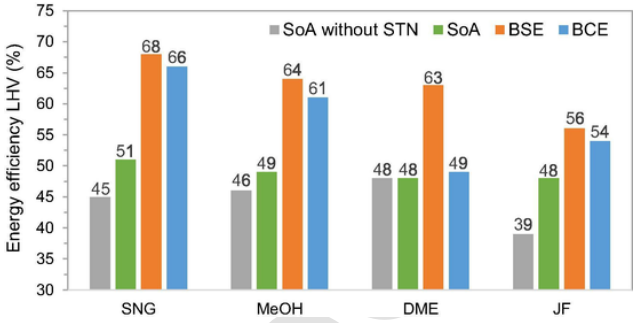

Fig. 7. The energy efficiency (LHV) of biomass-to-fuel systems with additional information, e.g., biomass consumption, the electricity consumption of electrolysis, imported electricity and stack number, given in Part B of the supplement material.

Along with the increase in the steps and complexity of chemical reaction and fuel upgrading, exergy destructions will be increased, leading to lower system energy efficiencies (e.g., SoA-JF without STN via LTFT reaches the lowest energy efficiency). Due to the mild exothermic reaction of MeOH dehydration to DME, SoA- and BCE-DME via MeOH-to-DME achieve similar energy efficiencies; however, BCE-DME case results in a lower energy efficiency due to additional requirement of hot utility (provided by syngas combustion with details referring to Section 4.1.2).

4.1.2. System-level heat integration

The integrated grand composite curves with the steam cycle are compared in Figs. 8–11. All processes except BCE-DME can realize heat self-sufficiency without hot utility, and the system efficiency can be enhanced by recovering excess heat via the steam cycle. The key parameters and size of optimal steam turbine and integrated composite curve are reported in Part B of the supplement material.

The BtSNG (Fig. 8a, b, and c) is the most exothermic case, due to the strongly exothermic CO and CO_2 methanation reactions. There is a large amount of heat released from the gasifier, syngas cooling, WGSR, SOE outlets, and methanation reactor, which is converted to power via the steam cycle. The steam extraction at a lower temperature after expansion is then used to supply the majority of heat required by the AGR and the steam generation for the SOE stacks. The H/C ratio of the methanation reaction is higher than those of methanol and LTFT synthesis, thus resulting in a larger stack number of BSE- and BCE-SNG. The heat demand for steam generation for the SOE stacks is about 1.5 and 2.6 times of that of BtMeOH and BtJF processes, respectively. For the SoA-SNG (Fig. 8a), since a large amount of CO is converted into CO_2 through a WGSR and removed via AGR, the heat released from the methanation reactor is only 34% of that of BSE-SNG (Fig. 8b). For the BCE-SNG (Fig. 8c), the captured CO_2 in SoA-SNG is fed into the SOE with H_2O via co-electrolysis to produce syngas required for SNG synthesis, thus similar heat release is obtained in the methanation reactor as the BSE-SNG. Since the BCE-SNG is still equipped with WGSR and AGR processes, a large amount of process heat is needed, leading to a lower energy efficiency.

For the BtMeOH (Fig. 9a, b, and c), although the methanolization reaction is less exothermic, the heat released from gasifier, recovery boiler, stack outlets and methanol reactor can still meet the heat de-

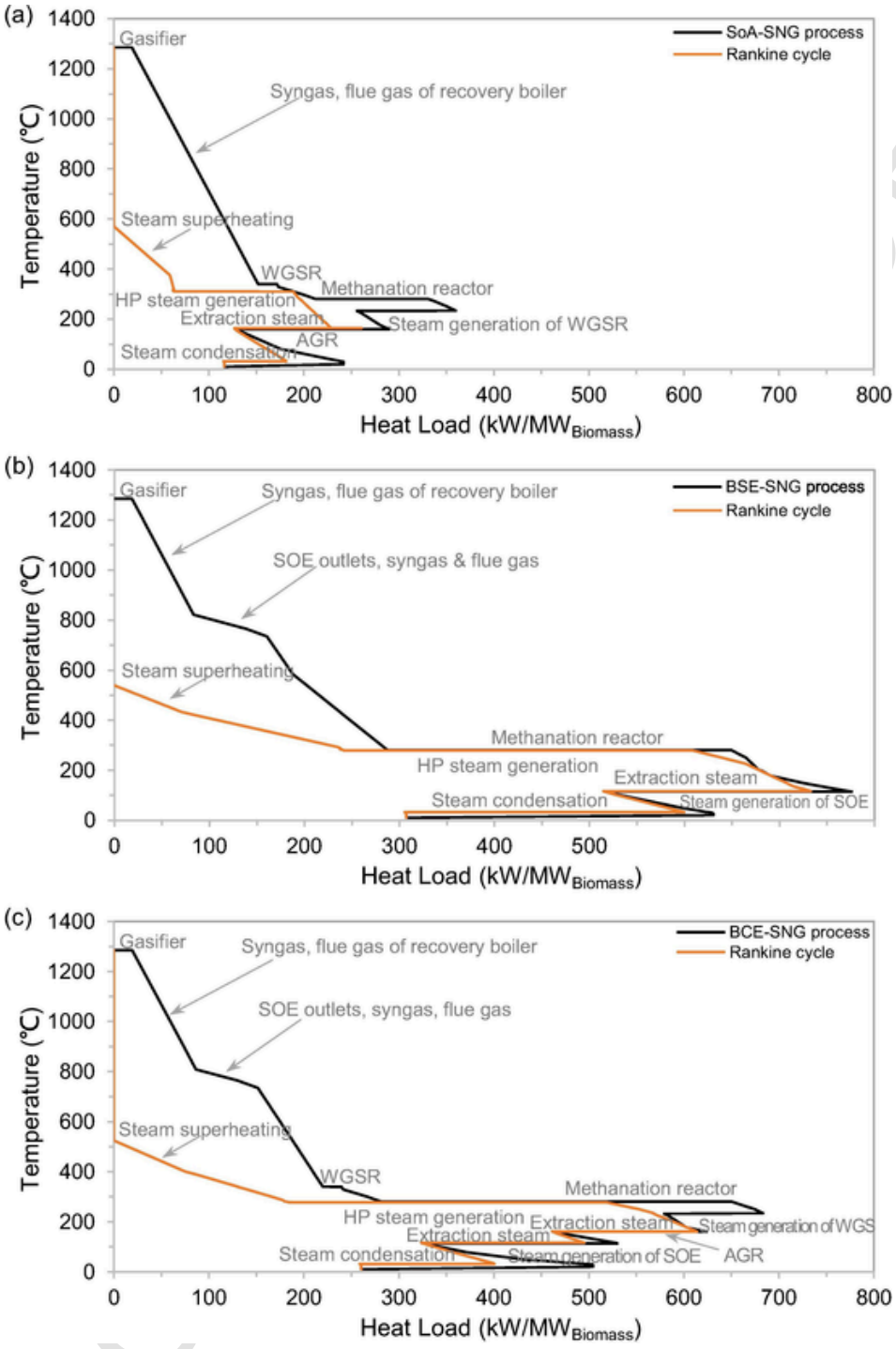

Fig. 8. Integrated composite curves of BtSNG with the yellow standing for the steam cycle and the black for the remaining process: (a) SoA-SNG, (b) BSE-SNG, (c) BCE-SNG.

mand of the steam generation for the stack and WGS, stack-inlet heating-up to 750 °C, AGR and two-stage distillation reboiler in three methanol processes. The remaining heat is recovered by the steam cycle to generate power.

The BtDME (Fig. 10a, b, and c) integrates methanol-to-DME based on BtMeOH, thus the gasification, recovery boiler, WGSR, AGR, SOE, and methanol synthesis processes are the same to BtMeOH. The additional heat released from methanol-to-DME is relatively small and has a limited impact on the overall heat integration. However, the column 3 for the DME purification is operated at 20 bar with the reboiler temperature being 210 °C, intensifying the heat integration below 230 °C. Hence, the net heat load presented in the grand composite curve is smaller than that of the BtMeOH. For the SoA-DME (Fig. 10a), compared to the SoA-MeOH, due to the energy consumption of DME purification, although the system can realize heat self-sufficiency, there is no excess heat available for the steam cycle. For the BSE-DME (Fig. 10b), due to the energy consumption of DME purification, excess heat of the BSE-DME is less than that of the BSE-MeOH, thus requiring a smaller steam cycle. The steam extraction from the steam turbine can partly meet the heat demand of steam generation for the stack, enhancing the cascade use of the heat of the energy pocket below 200 °C. For the BCE-DME (Fig. 10c), the system cannot realize heat self-sufficiency,

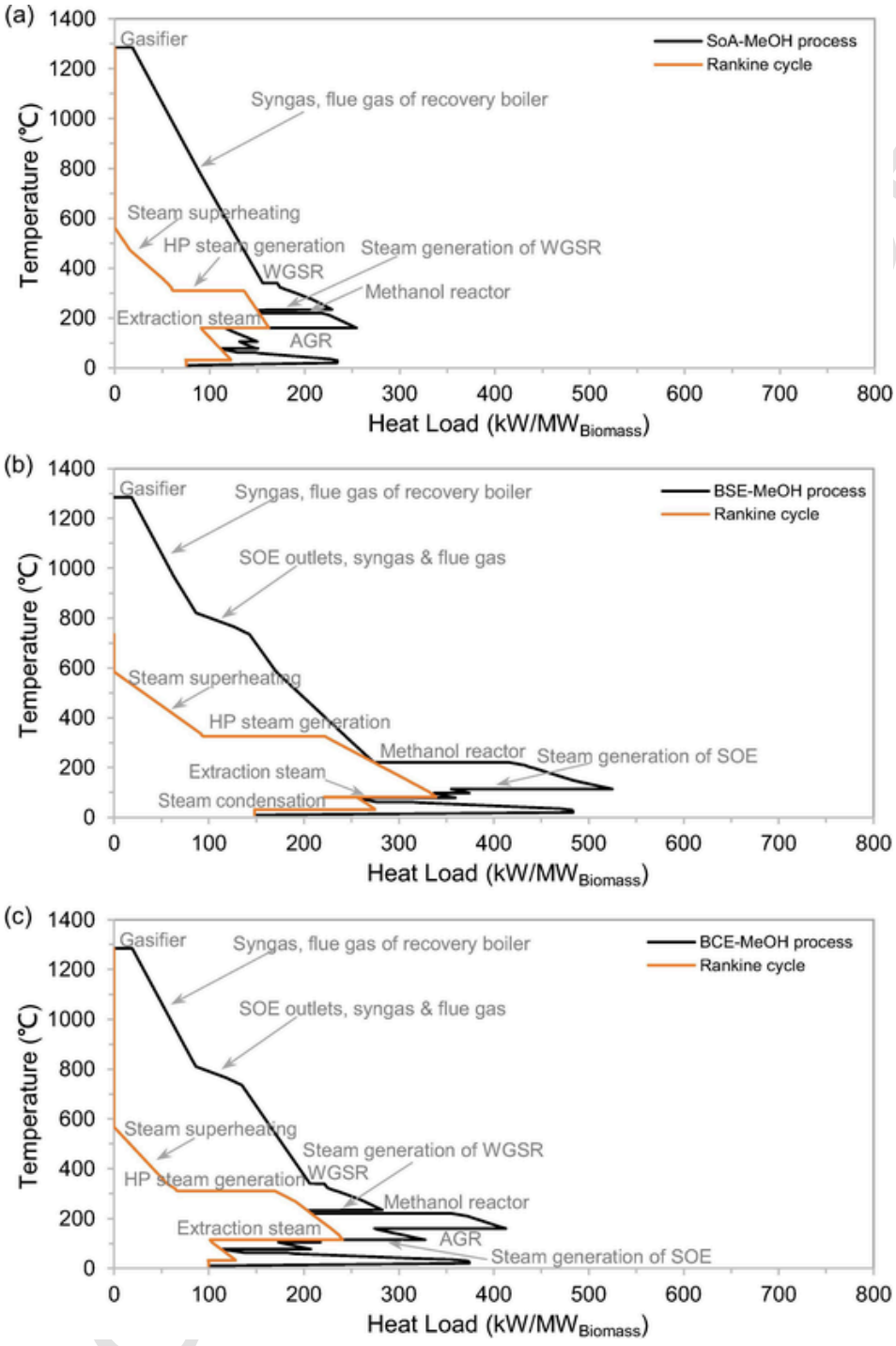

Fig. 9. Integrated composite curves of BtMeOH with the yellow standing for the steam cycle and the black for the remaining process: (a) SoA-MeOH, (b) BSE-MeOH, (c) BCE-MeOH.

and a part of syngas is sent to the auxiliary boiler to meet the heat gap, thus the energy efficiency of the BCE-DME is only 49% in Fig. 7.

For the BtJF (Fig. 11a, b, and c), the LTFT reaction is exothermic with the reaction heat between the methanolization and methanation reactions. Therefore, compared to the BtMeOH/DME, more excess heat can be recovered through the steam cycle. The BtJF has a large energy pocket above 200 °C, i.e., a lower level of heat cascade utilization, mainly because a large number of light hydrocarbons are recovered by the recovery boiler in the LTFT synthesis and upgrading process.

4.2. Economic performance

The economic indicators of the investigated cases are shown in Fig. 12 with more details on capital investment and economic assumptions given in Part A of the supplement material. Assuming a 25-year plant lifetime, 10% interest rate, 7200 annual operating hours (AoHs), 48,000 h stack lifetime [70], the stacks will be replaced 3 times for the whole plant lifetime, and the replacement cost is included in capital investment. The increase in the plant capacity will reduce the specific investment cost (Fig. 12a). For the three processes (SoA, BSE, BCE) with

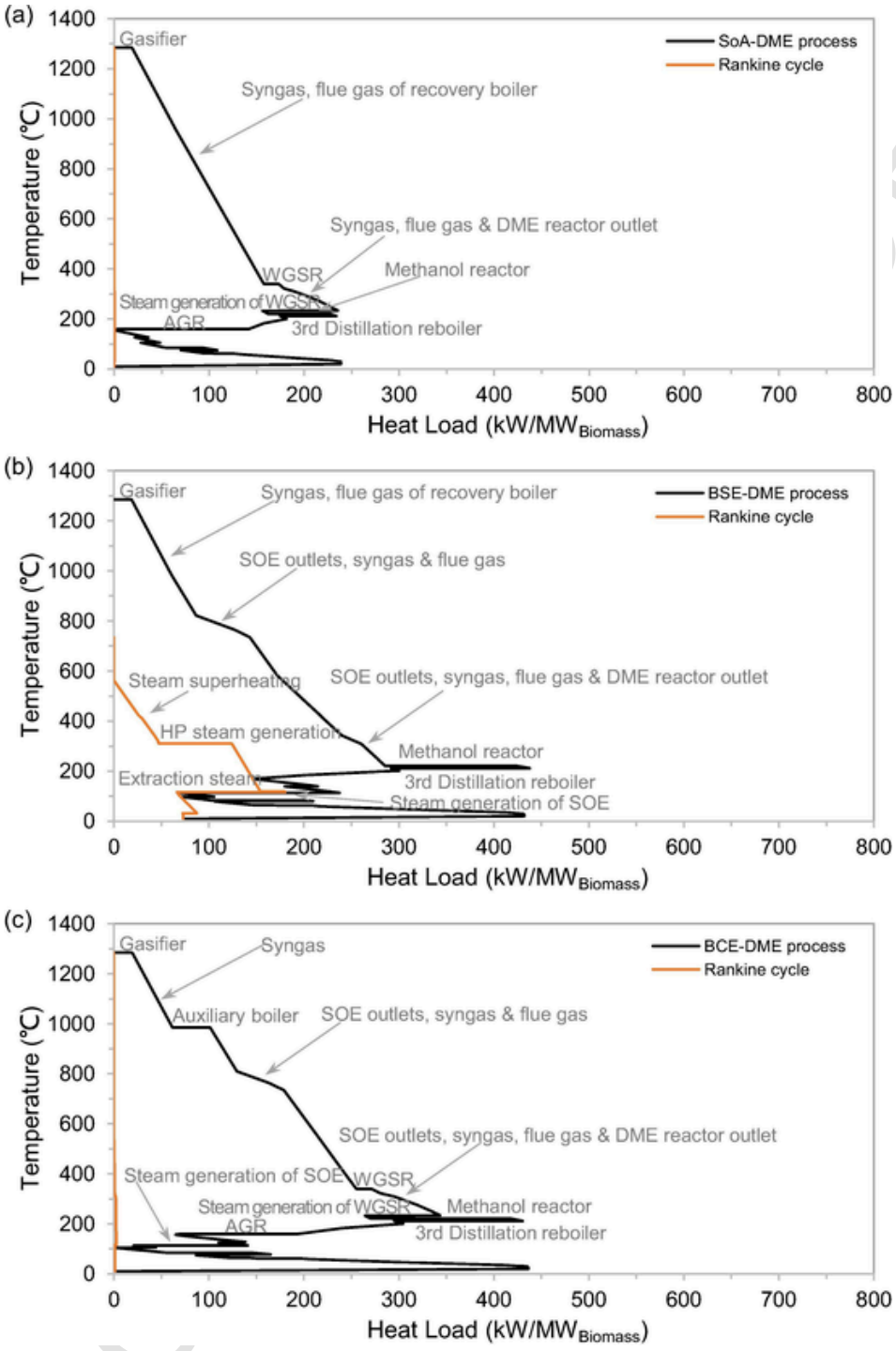

Fig. 10. Integrated composite curves of BtDME with the yellow standing for the steam cycle and the black for the remaining process: (a) SoA-DME, (b) BSE-DME, (c) BCE-DME.

the same product, the SoA process results in a higher specific CAPEX due to a lower fuel yield, followed by BCE and BSE processes. For instance, for the SNG production, the specific CAPEX ($/kW LHV product) is 3300 for SoA-SNG, 2341 for BCE-SNG, and 2208 for BSE-SNG for the scale of 60 MW_{th} biomass. While for different products, the specific CAPEX with 60 MW_{th} biomass input is calculated as follows: (1) For the SoA processes, the SoA-JF has the highest specific CAPEX (5169 $/kW), followed by SoA-SNG (3300 $/kW), SoA-MeOH (3206 $/kW), and SoA-DME (3046 $/kW) with the same order of magnitude. (2) For the BSE processes, the BSE-JF has the highest specific CAPEX (3880 $/kW), followed by BSE-DME (2315 $/kW), BSE-SNG (2208 $/kW), and BSE-MeOH (2062 $/kW) in the same order of magnitude. (3) For the BCE processes, the specific CAPEX has a similar variation trend to that of BSE. The specific CAPEX ($/kW LHV product) is 6–8 percentage points higher than those of the BSE for JF, SNG, and MeOH in 60 MW_{th} biomass, which is 21 percentage points higher than that of the BSE for DME.

The variation trend of levelized cost of the product (LCOP) along with plant capacity is similar to that of the specific CAPEX, as shown in Fig. 12b. For the same product, the SoA process can achieve the lowest

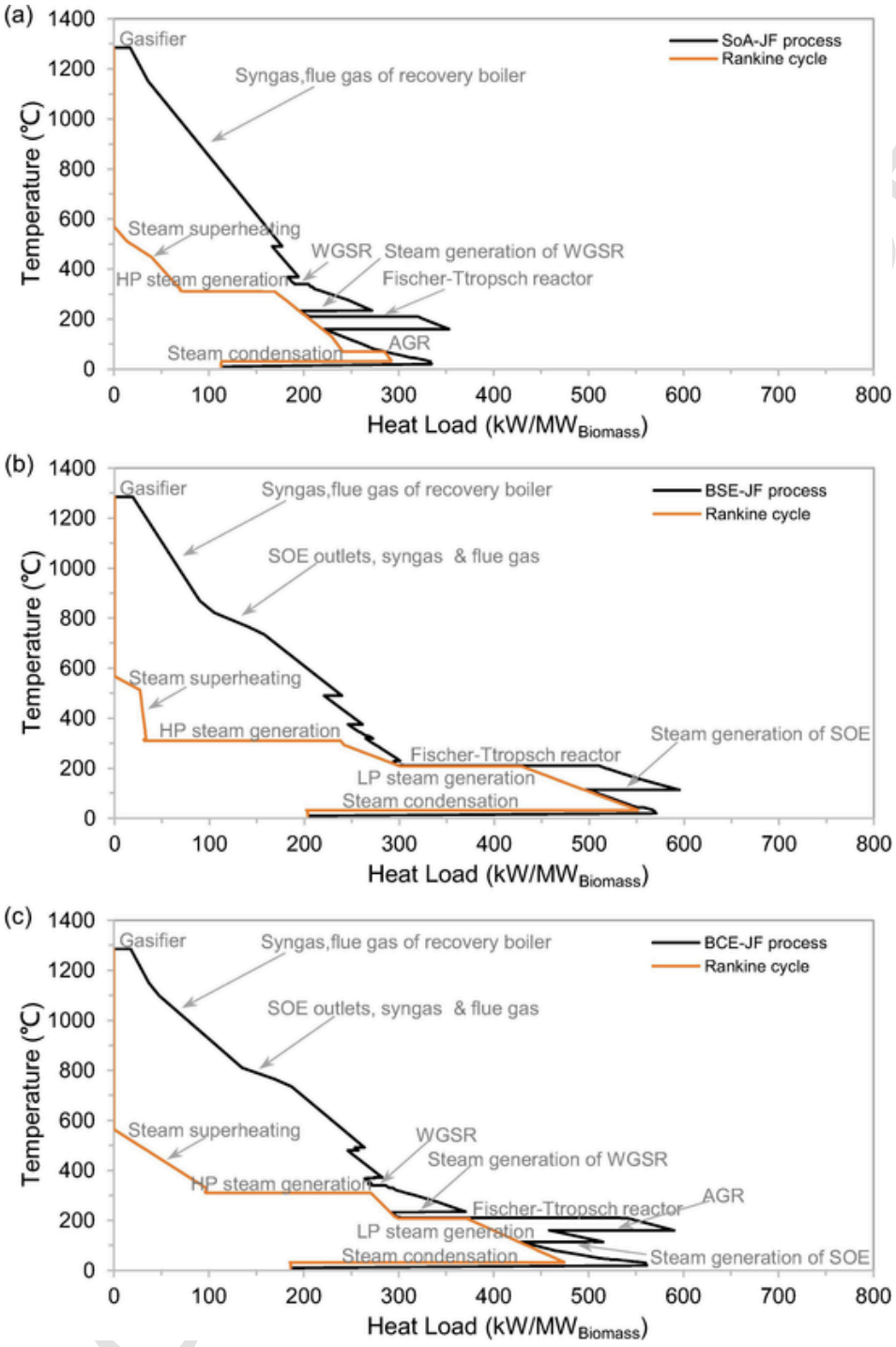

Fig. 11. Integrated composite curves of BtJF with the yellow standing for the steam cycle and the black for the remaining process: (a) SoA-JF, (b) BSE-JF, (c) BCE-JF.

LCOP, followed by the BSE and BCE. Taking the SNG production as an example, for the plant capacity of 10–60 MW_{th} biomass, the LCOP is 28–10 $/GJ for the SoA-SNG, 30–23 $/GJ for the BSE-SNG, and 32–26 $/GJ for the BCE-SNG. While for producing different products the LCOP of the plant with 10-60 MW_{th} biomass is also calculated: (1) For the SoA processes, the SoA-SNG has the lowest LCOP for the plant capacity of 10–45 MW_{th} biomass, followed by SoA-MeOH, SoA-DME, and SoA-JF. When the plant capacity increases from 45 to 60 MW_{th} biomass, the LCOP of SoA-JF is reduced to the level between that of SoA-MeOH and SoA-DME. The LCOP is 28–10 $/GJ for the SoA-SNG, 32–13 $/GJ for the SoA-MeOH, 35–16 $/GJ for the SoA-DME and 58–13 $/GJ for the SoA-JF. (2) For the BSE processes at the scale of 10–60 MW_{th} biomass, the BSE-SNG has the lowest LCOP (30–24 $/GJ), followed by BSE-MeOH (33–26 $/GJ), BSE-DME (37–28 $/GJ), and BSE-JF (59–39 $/GJ). (3) For the BCE processes at a scale of 10–60 MW_{th} biomass, the BCE-SNG has the lowest LCOP (33–26 $/GJ), followed by BCE-MeOH (36–28 $/GJ), BCE-DME (48–37 $/GJ), and BCE-JF (69–45 $/GJ). In order to be profitable, the products should be sold at a price higher than LCOP. For a payback time of 7 years, the minimum product selling price MPSP ($/GJ) is computed according to Ref. [66]. The trends of MPSP for different cases along with plant capacity are given in Fig. III of the supplement material.

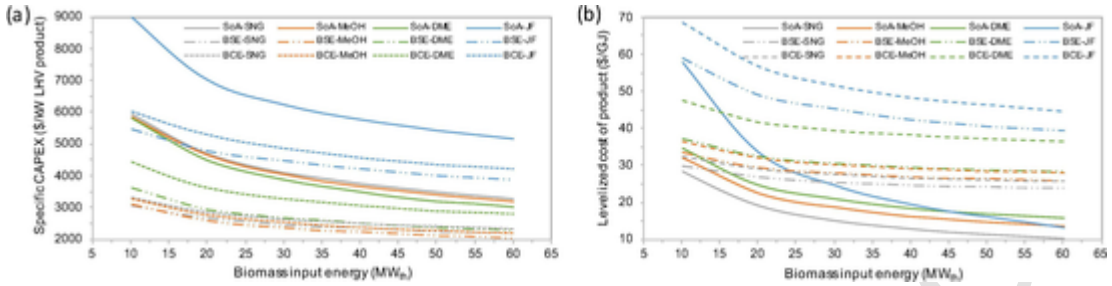

Fig. 12. The variation of economic indicators with plant capacity.

The SOE-based biomass-to-fuel systems require a large amount of renewable power to drive the SOE, thus both the price and available annual hours (AAHs) of renewable electricity have a significant impact on their economic feasibility. For the BSE-FUEL processes, when renewable electricity is not available, the plant needs to shut down due to the lack of large-scale storage of hydrogen and electricity. This means that the AAHs of the BSE-FUEL processes need to be equal to AOHs. For the BCE-FUEL processes, when renewable electricity is not available, the plant can still be operated in the SoA mode, while the captured CO_2 will be stored for use when renewable electricity is available. Thus, when the AAHs are smaller than AOHs, the system only needs to consider setting up the storage of CO_2 and O_2, which is considerably easier than the storage of hydrogen or electricity. Besides, in order to convert all captured CO_2, the size of SOE needs to be extended by AAHs/AOHs times.

Taking the BtSNG as an example (Fig. 13), when the AAHs are 7200 h, the LCOP of BCE-SNG is about 7% higher than that of the BSE-SNG. If the AAHs decrease from 7200 to 3600 and 1800 h with the electricity price being 73 $/MWh (Fig. 13a), the LCOP of BSE-SNG will increase by 23% and 91% for the plant of 60 MW_{th} biomass; however, the LCOP of the BCE-SNG will only increase by 16% and 27% for same plant size. With the decrease in AAHs, though the LCOP of both cases will increase, the increment of the LCOP of BSE-SNG is much higher than that of the BCE-SNG. When AAHs are 1800, the LCOP of BSE-SNG is 1.6–1.3 times of that of BCE-SNG for the scale of 10–60 MW_{th} biomass.

If the electricity price drops from 73 to 35 and 0 $/MWh with the AAHs of 7200 h, the operating cost will be decreased by 34% and 66%, leading to a decrease in LCOP of the BSE-SNG from 24 down to 16 and 8 $/GJ, and a decrease in LCOP of the BCE-SNG from 26 down to 17 and 9 $/GJ for the plant capacity with 60 MW_{th} biomass. The variation of the MPSP is given in Fig. IV of the supplement material.

4.3. Operational flexibility

Take the SNG production as an example, the operation of the SoA-SNG plant is mainly affected by the continuity of biomass supply, which can be easily avoided at the stage of site selection based on the current construction experience of biomass power plants. With the AOHs of 7200 h, the annual SNG production is 1.2×10^5 GJ with a biomass input of 10 MW_{th}.

According to results in section 4.1, the BSE-SNG plant can achieve the highest energy efficiency, but the system is greatly affected by renewable electricity. When renewable electricity is not available, the system must be shut down. Fig. 14 shows that when the AAHs are reduced to 3600 and 1800 h, respectively, the annual production of the SNG will be reduced by 50% and 75%, leading to a significant increase in LCOP of the BSE-SNG.

Compared to the BSE-SNG, the BCE-SNG is flexible in operation. When renewable electricity is not available, the SOE can disconnect from the system, the system maintains the SoA mode of operation without downtime, and stores the produced CO_2 for use in the periods with available renewable electricity. The plant can ensure stable and high annual production, with high operational flexibility.

5. Conclusions

In this study, different biomass-to-fuel processes (i.e., synthetic natural gas, methanol, dimethyl ether, jet fuel) are carried out via the integration of solid-oxide electrolyzer, aiming at evaluating their competitiveness systematically concerning thermodynamic and economic performances. The evaluation of each system considers system-level heat integration to close energy balance with the excess heat recovered by the steam cycle. Major conclusions include:

- The thermodynamic performances of biomass-to-fuels mainly depend on product synthesis and upgrading, system-level heat integration, and excess heat recovered by the steam cycle. Due to the low carbon conversion rates, the state-of-the-art biomass-to-fuel systems achieve the lowest energy efficiency (LHV): synthetic natural gas (51%), methanol (49%), dimethyl ether (48%), and jet fuel (48%). The biomass-to-fuel with steam electrolysis systems achieve the highest energy efficiency (LHV): synthetic natural gas (68%), methanol (64%), dimethyl ether (63%), and jet fuel (56%). By integrating the state-of-the-art biomass-to-fuel systems and co-electrolysis, all captured CO_2 can be converted with significantly increased efficiency (LHV): synthetic natural gas (66%), methanol (61%), and jet fuel (54%).

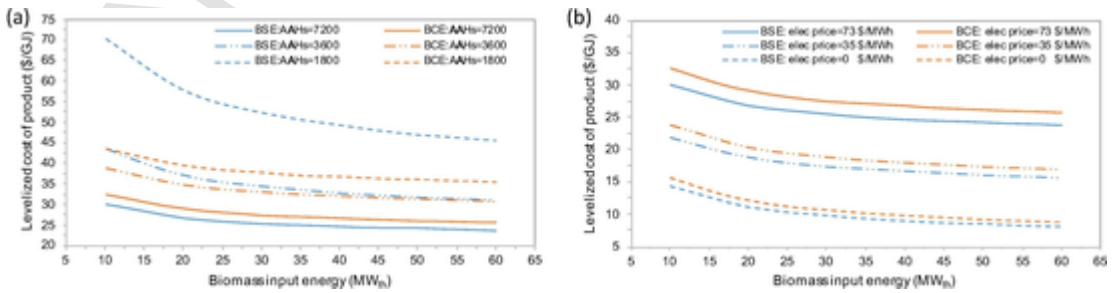

Fig. 13. Impacts of the electricity purchase price (0–73 $/MWh) and AOHs (1800–7200 h) on the LCOP of SNG.

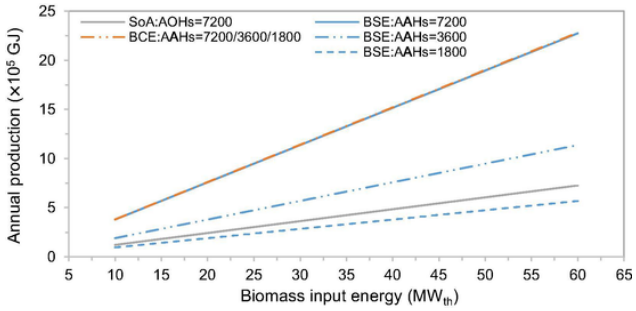

Fig. 14. Annual production with different AAHs.

- For producing the same fuel, state-of-the-art biomass-to-fuel can achieve the lowest levelized product cost, while that of the two integrated concepts highly depends on the price and availability of renewable electricity. The biomass-to-fuel with co-electrolysis has economic advantages. With 1800 annual available hours of renewable electricity, the levelized product cost of biomass-to-synthetic natural gas with steam electrolysis is 30–60% higher than the co-electrolysis concept for a plant with 10–60 MWth biomass.
- A lower price of renewable electricity can significantly reduce the levelized product cost. If it drops from 73 to 35 $/MWh with annual available hours of renewable electricity of 7200 h, the levelized product cost of biomass-to-synthetic natural gas with co-electrolysis will decrease from 26 to 17 $/GJ for a scale of 60 MWth biomass.
- Biomass-to-fuel with co-electrolysis can ensure continuous and high annual production with high operational flexibility. Biomass-to-fuel with steam electrolysis is greatly affected by renewable electricity. When renewable electricity is not available, the system might need to be shut down due to the lack of large-scale storage of hydrogen or electricity.

Credit authorship contribution statement

Hanfei Zhang: Conceptualization, Methodology, Validation, Investigation, Data curation. **Ligang Wang:** Methodology, Supervision. **Jan Van herle:** Methodology. **François Maréchal:** Methodology, Supervision. **Umberto Desideri:** Conceptualization, Supervision.

Declaration of Competing Interest

The authors declare that they have no known competing financial interests or personal relationships that could have appeared to influence the work reported in this paper.

Acknowledgments

The research leading to the above results was funded by China Scholarship Council, China, for the PhD scholarship of Mr. Hanfei Zhang and PRA2019 of the University of Pisa, Italy. Hanfei Zhang also thanks the group of Industrial Process and Energy Systems Engineering at EPFL for their support.

Appendix A. Supplementary material

Supplementary data to this article can be found online at https://doi.org/10.1016/j.apenergy.2020.115113.

References

[1] M Bukhtiyarova, T Lunkenbein, K Kähler, R Schlögl Methanol Synthesis from Industrial CO_2 Sources: A Contribution to Chemical Energy Conversion. Catal Lett 2017;147:416–427.
[2] G A Olah Beyond oil and gas: the methanol economy. Angew Chem Int Ed 2005;44:2636–2639.
[3] H Lin, H Jin, L Gao, W Han Techno-economic evaluation of coal-based polygeneration systems of synthetic fuel and power with CO_2 recovery. Energy Convers Manage 2011;52:274–283.
[4] I S Tagomori, P Rochedo, A Szklo Techno-economic and georeferenced analysis of forestry residues-based Fischer-Tropsch diesel with carbon capture in Brazil. Biomass Bioenergy 2019;123:134–148.
[5] S R Naqvi, S Jamshaid, M Naqvi, W Faroop, M Niazi, A Aman, et al. Potential of biomass for bioenergy in Pakistan based on the present case and future perspectives. Renew Sustain Energy Rev 2018;81:1247–1258.
[6] World Energy Council report. World energy resources bioenergy; 2016.
[7] L Tock, M Gassner, F Maréchal Thermochemical production of liquid fuels from biomass: Thermo-economic modeling, process design and process integration analysis. Biomass Bioenergy 2010;34:1838–1854.
[8] M Gassner, F Maréchal Thermo-economic optimization of the polygeneration of synthetic natural gas (SNG), power and heat from lignocellulosic biomass by gasification and methanation. Energy Environ Sci 2012;5:5768.
[9] E Steen, M Claeys Fischer-Tropsch catalysts for the biomass-to-liquid process. Chem. Eng. Technol 2008;5:655–666.
[10] U Wolfesberger, I Aigner, H Hofbauer Tar content and composition in producer gas of fluidized bed gasification of wood-influence of temperature and pressure. Environ Prog Sustainable Energy 2009;28:372–379.
[11] Zhang H, Wang L, Pérez-Fortes M, Van herle J, Maréchal F, Desideri U. Techno-economic optimization of biomass-to-methanol with solid-oxide electrolyzer. Appl Energy 2020;258:114071.
[12] A Valero, S Uson Oxy-co-gasification of coal and biomass in an integrated gasification combined cycle (IGCC) power plant. Energy 2006;31:1643–1655.
[13] A Minchener Coal gasification for advanced power generation. Fuel 2005;84:2222–2235.
[14] K Qin Entrained flow gasification of biomass Ph.D. thesis. Technical University of Denmark; 2012.
[15] S S Santiago High temperature gasification of millimetric wood particles between 800°C and 1400°C Ph.D. thesis. University of Toulouse; 2011.
[16] C Higman, M Van der Burgt Gasification. Burlington: Gulf Professional Publishing; 2008.
[17] M Ostadi, E Rytter, M Hillestad Boosting carbon efficiency of the biomass to liquid process with hydrogen from power: The effect of H_2/CO ratio to the Fischer-Tropsch reactors on the production and power consumption. Biomass Bioenergy 2019;127:105282.
[18] Dutcher B, Fan M, Russell A.G. Amine-Based CO2 Capture Technology Development from the Beginning of 2013 - A Review. Appl Mater Interfaces 2015;7:2137–2148.
[19] A Duret, C Friedli, F Maréchal Process design of synthetic nature gas (SNG) production using wood gasification. J Cleaner Prod 2005;13:1434–1446.
[20] I Dimitriou, H Goldingay, A Bridgwater Techno-economic and uncertainty analysis of biomass to liquid (BtL) system for transport fuel production. Renew Sustain Energy Rev 2018;88:160–175.
[21] C Hamelinck, A Faaij, H Uil, H Boerrigter Production of FT transportation fuels from biomass; technical options, process analysis and optimization, and development potential. Energy 2004;29:1743–1771.
[22] G Botta, M Solimeo, P Leone, P V Aravind Thermodynamic Analysis of Coupling a SOE in Co-Electrolysis Mode with the Dimethyl Ether Synthesis. Fuel Cells 2015;15:669–681.
[23] The future of petrochemicals. International Energy Agency; 2018.
[24] Zhang H, Wang L, Van herle J, Maréchal F, Desideri U. Techno-economic comparison of green ammonia production processes. Applied Energy 2020;259:114135.
[25] L Clausen, G Butera, S Jensen High efficiency SNG production from biomass and electricity by integrating gasification with pressurized solid oxide electrolysis cells. Energy 2019;172:1117–1131.
[26] Z Pan, W Chan, A Veksha, A Giannis, X Dou, H Wang, et al. Thermodynamic analyses of synthetic nature gas production via municipal solid waste gasification, high-temperature water electrolysis and methanation. Energy Convers Manage 2019;201:112160.
[27] E Peduzzi, G Boissonnet, G Haartemmer, F Marechal Thermo-economic analysis and multi-objective optimisation of lignocellulosic biomass conversion to Fischer-Tropsch fuels. Sustain Energy Fuels 2018;2:1069–1084.
[28] L Wang, M Chen, R Kungas, T E Lin, S Diethelm, F Maréchal, et al. herle J. Power-to-fuels via solid-oxide electrolyzer: Operating window and techno-economics. Renew Sustain Energy Rev 2019;110:174–187.
[29] P Kazempoor, R J Braun Hydrogen and synthetic fuel production using high temperature solid oxide electrolysis cells (SOECs). Int J Hydrogen Energy 2015;40:3599–3612.
[30] J B Hansen Solid oxide electrolysis–a key enabling technology for sustainable energy scenarios. Faraday Discuss 2015;182:9–48.
[31] N Gallandat, R Mutschler, V Vernay, H Yang, A Zuttel Experimental performance investigation of a 2 kW methanation reactor. Sustain Energy Fuels 2018;2(5):1101–1110.
[32] J Gao, Q Liu, F Gu, B Liu, Z Zhong, F Su Recent advances in methanation catalysts for the production of synthetic natural gas. RSC Adv 2015;5(29):22759–22776.
[33] R Turton, R C Bailie, W B Whiting, J A Shaeiwitz Analysis synthesis and design of chemical processes. Pearson Education; 2008.
[34] M Rao, X Sun, A Hagen Long term testing of solid oxide electrolysis cells under Co-electrolysis conditions. ECS Trans 2017;80(9):57–69.

[35] Wang L, Pérez-Fortes M, Madi H, Diethelm S, Van Herle J, Maréchal F. Optimal design of solid-oxide electrolyzer based power-to-methane systems: A comprehensive comparison between steam electrolysis and co-electrolysis. Appl Energy 2018;211:1060–1079.
[36] Jeanmonod G, Wang L, Pérez-Fortes M, Diethelm S, Maréchal F, Van Herle J. Trade-off designs of power-to-methane via solid-oxide electrolyzer swept by oxygen: application to biogas upgrading. Appl Energy 2019;247:572–581.
[37] L Wang, R Megha, S Diethelm, L Tzu-En, Z Hanfei, F Maréchal Power-to-methane via co-electrolysis of H_2O and CO_2: Process modeling, pressurized operation and internal methanation. Appl Energy 2019;250:1432–1445.
[38] Wang L, Johannes D, Maréchal F, Van Herle J. Trade-off designs and comparative exergy evaluation of solid-oxide electrolyzer based power-to-methane plants. Int J Hydrogen Energy 2018;44:9529–9543.
[39] J B Hansen, P E H Nielsen Handbook of Heterogeneous Catalysis. Wiley-VCH Verlag; 2008.
[40] P Tijm, F Waller, D Brown Methanol technology developments for the new millennium. Appl Catal A 2001;221:275–282.
[41] Wilkinson S, Water L, Miller B, Simmons M, Still E, Watson M. Understanding the generation of methanol synthesis and water gas shift activity over copper-based catalysts – A spatially resolved experimental kinetic study using steady and non-steady state operation under CO/CO2/H2 feeds. J Catal 2016;337:208–20.
[42] C S Bildea, R Győrgy, C C Brunchi, A A Kiss Optimal design of intensified processes for DME synthesis. Comput Chem Eng 2017;105:142–151.
[43] D Mao, W Yang, J Xia, B Zhang, G Lu The direct synthesis of dimethyl ether from syngas over hybrid catalysts with sulfate-modified ϒ-alumina as methanol dehydration components. J Mol Catal A: Chem 2006;250:138–144.
[44] M Ateah, G Ahmed, A Almadani, A Ba-Shammakh, S Noaman, M Qasem Manufacturing of DME from methanol. CHE 495-Senior Design Project. Final Report. King Fahd University of Petroleum and Minerals; 2014–2015..
[45] T Semelsberger, R Borup, H Greene Dimethyl ether (DME) as an alternative fuel. J Power Sources 2006;156:497–511.
[46] D Selvatico, A Lanzini, M Santarelli Low temperature Fischer-Tropsch from syngas: Kinetic modeling and process simulation of different plant configurations. Fuel 2016;58:267–286.
[47] Klerk A. Fischer-Tropsch Refining. Wiley-VCH verlag; 2011.
[48] S S Ail, S Dasappa Biomass to liquid transportation fuel via Fischer Tropsch synthesis – Technology review and current scenario. Renew Sustain Energy Rev 2016;58:267–286.
[49] Lualdi M. Fischer-Tropsch synthesis over cobalt-based catalysts for BTL applications. Ph.D. thesis. KTH chemical science and engineering; 2012.
[50] S Spyrakis, K D Panopoulos, E Kakaras Synthesis, modeling and exergy analysis of atmospheric air blown biomass gasification for Fischer-Tropsch process. Int J Thermodyn 2009;12:187–192.
[51] C Schnuelle, J Thoeming, T Wassermann, P Thier, A V Gleich, S Goessling-Reisemann Socio-technical-economic assessment of power-to-X: Potentials and limitations for an integration into the German energy system. Energy Res Social Sci 2019;51:187–197.
[52] Z Navas-Anguita, P L Cruz, M Martín-Gamboa, D Iribarren Simulation and life cycle assessment of synthetic fuels produced via biogas dry reforming and Fischer-Tropsch synthesis. Fuel 2019;235:1492–1500.
[53] Z T Lv Study on life cycle assessment of bio-vehcile and bio-aviation fuel production system based on exergy theory. Master thesis. China: Southeast University; 2017.
[54] A Klerk Fischer-Tropsch fuels refinery design. Energy Environ Sci 2011;4:1177.
[55] Sakuneka TM, Klerk A, Nel R, D. Pienaar A. Synthetic Jet Fuel Production by Combined Propene Oligomerization and Aromatic Alkylation over Solid Phosphoric Acid. Ind Eng Chem Res 2008;47:1828–1834.
[56] N Belinskaya, E Ivanchina, E Ivashkina, E Frantsina, G Silko Mathematical model of straight run diesel catalytic hydroisomerization. IOP Conf. Series: Earth and Environmental. Science 2014;21:12030.
[57] H Zhang, L Wang, F Maréchal, U Desideri Solid-oxide electrolyzer coupled biomass-to-methanol systems. Energy Procedia 2019;158:4548–4553.
[58] G Cinti, A Baldinelli, A Di Michele, U Desideri Integration of Solid Oxide Electrolyzer and Fischer-Tropsch: A sustainable pathway for synthetic fuel. Appl Energy 2016;162:308–320.
[59] M Gassner Process design methodology for thermochemical production of fuels from biomass. Appliaction to the production of synthetic natural gas from lignocellulosic resources Ph.D. thesis. École Polytechnique Fédérale de Lausanne; 2010.
[60] F Maréchal, B Kalitventzeff Process integration: Selection of the optimal utility system. Comput Chem Eng 1998;22:149–156.
[61] F Maréchal, B Kalitventzeff Targeting the optimal integration of steam networks. Comput Chem Eng 1999;23:133–136.
[62] A S Wallerand, M Kermani, I D Kantor, F Maréchal Optimal heat pump integration in industrial processes. Appl Energy 2018;219:68–92.
[63] M Kermani, A S Wallerand, I D Kantor, F Maréchal Generic superstructure synthesis of organic Rankine cycles for waste heat recovery in industrial processes. Appl Energy 2018;212:1303–1225.
[64] Zhang H, Wang L, Van herle J, Maréchal F, Desideri U. Techno-Economic Optimization of CO2-to-Methanol with Solid-Oxide Electrolyzer. Energies 2019;12:3742.
[65] A Mian Optimal design methods applied to solar-assisted hydrothermal gasification plants Ph.D. thesis. École Polytechnique Fédérale de Lausanne; 2016.
[66] J Q Albarelli, S Onorati, P Caliandro, E Peduzzi, M Meireles, F Maréchal, et al. Multi-objective optimization of a sugarcane biorefinery for integrated ethanol and methanol production. Energy 2017;138:1281–1290.
[67] Yankuang Xinjiang methanol and ammonia project in China.
[68] Energy DG. Quarterly report on European electricity markets, fourth quarter of 2017. European Commission.
[69] G Haarlemmer, G Boissonnet, J Imbach, P A Setier, E Peduzzi Second generation BtL type biofuel – a production cost analysis. Energy Environ Sci 2012;5:8445–8456.
[70] O Schmidt, A Gambhir, I Staffell, A Hawkes, J Nelson, S Few Future cost and performance of water electrolysis: An expert elicitation study. Int J Hydrogen Energy 2017;42:30470–30492.